Research Article

Journal of Environmental Nanotechnology

Green Synthesis and Biomedical Evaluation of *Pergularia daemia*-Functionalized ZnO/P4VP Nanocomposite

S. S. Sandheep[1], Gulipalli Pallavi[2] and Sorimuthu Revathi[3]*

[1]Department of undergraduate Medical Education, Saveetha Medical College and Hospital, Saveetha Institute of Medical and Technical Sciences, Chennai, TN, India

[2]Department of General Medicine, Saveetha Medical College and Hospital, Saveetha Institute of Medical and Technical Sciences, Chennai, TN, India

[3]Department of Emergency Medicine, Saveetha Medical College and Hospital, Saveetha Institute of Medical and Technical Sciences, Chennai, TN, India

Received: 16.07.2026 Accepted: 18.08.2026 Published: xx.xx.xxxx

*revathis1598@gmail.com

ABSTRACT

Green synthesis of polymer-functionalized metal oxide nanocomposites has emerged as a sustainable approach for developing materials with improved stability and biological activity. Zinc oxide nanoparticles combined with medicinal plant phytochemicals and polymer matrices offer potential antimicrobial properties while improving nanoparticle dispersion and biocompatibility. Although *Pergularia daemia* possesses diverse bioactive phytochemicals and ZnO nanoparticles exhibit antimicrobial activity, limited studies have explored *Pergularia daemia*-functionalized ZnO/poly(4-vinylpyridine-co-styrene) (PD-Zn@P4VP NC) and their physicochemical characteristics and *in vitro* biological properties. PD-Zn@P4VP NC were synthesized using an aqueous extract of *P. daemia* and characterized by UV–Visible spectroscopy, FTIR, FESEM–EDX, XRD, dynamic light scattering (DLS), and zeta potential analysis. Antibacterial activity was evaluated against *Staphylococcus aureus* and *Klebsiella pneumoniae* using the agar well diffusion method, while cytocompatibility was assessed in HFF-2 fibroblast cells using the MTT assay. The synthesized nanocomposite exhibited a characteristic UV–Visible absorption peak at 372 nm, confirming ZnO formation. DLS analysis showed an average hydrodynamic particle size of 280.8 nm, with a zeta potential of 32.15mV, indicating good colloidal stability. The nanocomposite showed concentration-dependent antibacterial activity, producing inhibition zones of 19 mm against *Staphylococcus aureus* and 20 mm against *Klebsiella pneumoniae* at 100 µg/mL. Cytocompatibility studies demonstrated approximately 69% cell viability in HFF-2 cells at 100 µg/mL. The PD-Zn@P4VP NC exhibited favorable physicochemical properties, antibacterial activity, and acceptable *in vitro* cytocompatibility. These findings provide a basis for further mechanistic investigations, evaluation against additional microbial strains, and *in vivo* studies to determine its safety and therapeutic potential.

Keywords: *Pergularia daemia;* Zinc oxide nanoparticles; Poly(4-vinylpyridine-co-styrene); Cytocompatibility; Medicine.

1. INTRODUCTION

One of the biggest threats to global public health today is antimicrobial resistance (AMR), leading to increased morbidity, mortality, and healthcare costs worldwide. Global health estimates attribute approximately 700,000 annual deaths to AMR infections; the increase is projected to approach 10 million by 2050 with effective interventions(Ahmed *et al.* 2024). The rapid emergence of multidrug-resistant infections have dramatically decreased the efficacy of traditional antibiotics, necessitating innovative materials with improved efficacy and reduced resistance risk(Elshobary *et al.* 2025). Because of the special physicochemical characteristics of nanoparticles, such as their high surface area to volume ratio, increased reactivity, and capacity to damage microbial membranes through the production of reactive oxygen species and release of metal ions, nanotechnology has become a promising strategy(Hetta *et al.* 2023). Cancer keeps being one of the world's leading causes of death and a significant global health burden. Despite remarkable advances in chemotherapy, radiotherapy, and targeted therapies, conventional treatment is limited by severe side effects, poor selectivity, multidrug resistance, and damage to healthy tissues(Zafar *et al.* 2025). Consequently, considerable research has focused on developing nanomaterial-based therapeutic systems that minimize harm to healthy cells while specifically targeting malignant cells. Metal oxide Nps have demonstrated considerable potential in this regard because of their unique optical, electronic, and biological properties that enable enhanced cellular uptake, oxidative stress induction, DNA damage, apoptosis, and mitochondrial malfunction in malignant cells(Elumalai *et al.* 2023; Sidhic *et al.* 2025).

Among various metal oxide nanomaterials, ZnO Nps are promising AA and cytocompatibility therapies due to their excellent biocompatibility, chemical stability, low cost, and multifunctional biological activities. The broad-spectrum is effective against both Gram-positive and Gram-negative bacteria antibacterial action of ZnO Nps through multiple mechanisms, including disruption of bacterial cell membranes, intracellular reactive oxygen species generation, release of Zn^{2+} ions, and interference with essential cellular metabolic pathways(Dada *et al.* 2026). Furthermore, it has demonstrated cytotoxic effects against various cancer cell lines through inducing oxidative stress, mitochondrial membrane depolarization, apoptotic signalling pathways, and cell cycle arrest while exhibiting comparatively lower toxicity toward normal cells. ZnO Nps promising candidates for biomedical applications, particularly in antimicrobial and cytocompatibility (Vagena *et al.* 2024; Xie *et al.* 2023). Although ZnO NPs possess remarkable biological properties, their biomedical applications are often restricted by NPs aggregation, limited colloidal stability, and uncontrolled release of metal ions under physiological conditions. Surface functionalization using polymeric materials has proven to be an effective strategy for overcoming these limitations. Polymeric matrices improve NPs dispersion, enhance physicochemical stability, minimize aggregation, and provide functional groups for immobilization of bioactive molecules. In addition, polymer-assisted NCs improve biocompatibility, prolong biological stability, and sustain interaction with target cells, thereby enhancing therapeutic efficacy(Sharma *et al.* 2019; Vagena *et al.* 2024).

Poly(4-vinylpyridine-co-styrene) (P4VP) is an attractive copolymer for NC fabrication because it combines the structural rigidity of styrene with the chemically active pyridine functional groups of poly(4-vinylpyridine). The pyridine moieties exhibit strong coordination with metal ions and NPs surfaces, enabling efficient stabilization of ZnO NPs while preventing particle agglomeration(Gal *et al.* 2011). In addition, the polymer matrix can improve nanoparticle dispersion and provide binding sites for plant-derived phytochemicals (Constantino *et al.* 2023). Although several plant-mediated ZnO nanoparticles have been reported using medicinal plant extracts as reducing and capping agents, most studies have primarily focused on unmodified ZnO nanoparticles or ZnO stabilized with conventional polymers such as polyvinylpyrrolidone (PVP), polyethylene glycol (PEG), and chitosan (Ramachandran *et al.* 2023). These systems have demonstrated improved nanoparticle stability and biological activity; however, the incorporation of a pyridine-functionalized copolymer such as poly(4-vinylpyridine-co-styrene) (P4VP) provides an additional functional advantage because the pyridine groups can interact with metal-containing surfaces while the polymer matrix contributes to steric stabilization and improved dispersion (Gal *et al.* 2011). In comparison with conventional polymeric stabilizers, P4VP therefore offers the possibility of simultaneously providing nanoparticle stabilization and chemically active functional sites for interaction with plant-derived phytochemicals.

Importantly, the combined use of *Pergularia daemia* phytochemicals, ZnO, and P4VP has received very limited attention. Previous plant-mediated ZnO studies have generally investigated the biological properties of ZnO nanoparticles alone or used different polymeric matrices, whereas systematic studies integrating *P. daemia* phytochemicals with ZnO within a P4VP copolymer matrix are scarce. Furthermore, the influence of this three-component combination on nanoparticle crystallinity, surface characteristics, hydrodynamic stability, antibacterial activity, and compatibility toward normal fibroblast cells has not been comprehensively established. Therefore, the novelty of the present work lies in the development of a plant–metal oxide–functional copolymer hybrid, in which *P. daemia* phytochemicals provide biological functionality and surface capping, ZnO provides the inorganic antimicrobial component, and P4VP provides polymeric stabilization and dispersion. This integrated design distinguishes PD-Zn@P4VP from conventional plant-mediated ZnO nanoparticles and commonly reported PVP- or PEG-stabilized ZnO systems.

Pergularia daemia (Forssk.) Chiov., a perennial medicinal climber belonging to the family Asclepiadaceae, has been widely used to treat fever in traditional medicine, pain, skin disorders, respiratory diseases, rheumatism, and microbial infections(Ananth *et al.* 2021). Phytochemical investigations have demonstrated that is rich in Alkaloids, terpenoids, flavonoids, phenolic compounds, saponins, tannins, and glycosides many of which possess potent antioxidant, antimicrobial, cytoprotective, and cytocompatibility activities(Ananth *et al.* 2016). Many more pharmacological studies have confirmed the AA of *P. daemia* extracts against a wide range of pathogenic microorganisms and their capacity to scavenge reactive oxygen species, preventing oxidative damage to cells. These bioactive phytochemicals can also function as natural reducing, capping, and stabilizing agents during green synthesis Nps, eliminating the need for hazardous chemical reagents and improving the biological compatibility of the synthesized nanomaterials(Kavaye *et al.* 2021).

Green synthesis has emerged as an environmentally friendly to conventional chemical synthesis of NPs(Ehisuoria *et al.* 2025). Green synthesis utilizes naturally occurring phytochemicals to reduce metal precursors and simultaneously stabilize the synthesized NPs demonstrated in enhanced biological functionality, reduced toxicity, and improved

environmental compatibility(Herin *et al.* 2025; Vaithiyanathan and Mirunalini, 2015). Functionalization of ZnO NPs with medicinal plant extracts within a polymeric matrix has emerged as an effective strategy to improve nanoparticle stability, dispersion and biological performance by combining the intrinsic antimicrobial properties of ZnO with the therapeutic potential of plant-derived phytochemicals and the stabilizing effect of functional polymers (Herin *et al.* 2025; Ramachandran *et al.* 2023). Previous studies have mainly focused on polymer-coated ZnO nanocomposites employing polymers such as polyvinylpyrrolidone (PVP), chitosan, and polyethylene glycol to enhance physicochemical stability and antimicrobial performance. However, the use of poly(4-vinylpyridine-co-styrene) (P4VP) as a functional polymer together with the medicinal plant *Pergularia daemia* has received little attention. Accordingly, the present study aimed to synthesize *Pergularia daemia*-functionalized ZnO/P4VP nanocomposites using a green synthesis approach and systematically investigate their structural, optical, morphological, colloidal, antibacterial, and cytocompatibility properties. The study specifically evaluates antibacterial activity against *Staphylococcus aureus* and *Klebsiella pneumoniae* and cytocompatibility toward HFF-2 normal human fibroblast cells. The resulting findings provide a basis for understanding the contribution of the plant extract and P4VP matrix to the physicochemical stability and biological performance of the ZnO nanocomposite.

2. MATERIALS AND METHODS

2.1 Materials

Zinc acetate dihydrate [$Zn(CH_3COO)_2 \cdot 2H_2O$] (99.9%) and poly(4-vinylpyridine-co-styrene) (P4VP) were purchased from Himedia. Ethanol (99.9% grade) and distilled water were used throughout the study. *Pergularia daemia* plant material was obtained from a commercially available herbal source.

2.2 Preparation *of Pergularia daemia* Aqueous Extract

Powdered PD dired leaf was made. In short, 150 mL of DM and 10 g of powdered PD were mixed, and the solution was heated to 60°C for 30 to 50 minutes while being continuously stirred. Whatman No. 1 filter paper was used to filter the mixture once it had cooled to room temperature. The resulting filtrate was gathered and kept at 4 °C until it was needed for NPs.

2.3 Green Synthesis of *Pergularia daemia*-Functionalized ZnO/P4VP Nanocomposite

Initially, a 0.063 M solution of zinc acetate dihydrate [$Zn(CH_3COO)_2 \cdot 2H_2O$] was prepared by dissolving the required amount of zinc acetate dihydrate in 500 mL of distilled water. Separately, 0.5 g of poly(4-vinylpyridine-co-styrene) (P4VP) was dissolved in 50 mL of ethanol to obtain a clear polymer solution. The P4VP solution was added slowly to the zinc acetate solution under continuous magnetic stirring. Subsequently, 20 mL of the prepared *Pergularia daemia* (PD) aqueous leaf extract was added dropwise while maintaining constant stirring. The reaction mixture was maintained at pH 8.0–9.0 without further pH adjustment and continuously stirred until a stable milky-white suspension was obtained. The gradual change from a clear solution to a milky-white suspension indicated the formation of the ZnO-based nanocomposite. The resulting suspension was centrifuged at 5000 rpm for 15 min to collect the formed nanocomposite. The precipitate was washed three times with distilled water, followed by ethanol washing, to remove unreacted precursors and loosely bound impurities. The purified precipitate was dried in a hot-air oven at 60 °C for 24 h, followed by gentle grinding to obtain a fine powder. The optimized synthesis yielded approximately 1.27 g of dried PD-Zn@P4VP nanocomposite**,** which was stored in airtight containers until further physicochemical characterization and biological evaluation (Song *et al.* 2021). The synthesis procedure is schematically illustrated in Fig. 1. The formation of the white precipitate was consistent with previously reported green synthesis of ZnO nanostructures using plant-derived materials (Gutul *et al.* 2014).

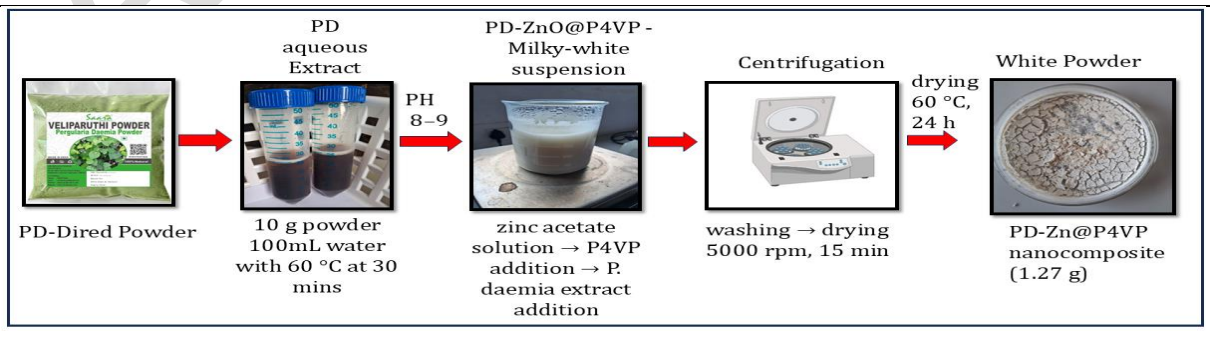

Fig. 1: Schematic representation of the green synthesis of the PD-Zn@P4VP nanocomposite

2.4 Characterization of *Pergularia daemia*-Functionalized ZnO/P4VP Nanocomposite

The synthesized PD-ZnO@P4VP NC was characterized using various analytical techniques to investigate optical, structural, morphological, elemental, and physicochemical properties.

2.4.1 UV–Visible Spectroscopy

A UV- visible spectrophotometer operating in the 200–800 nm wavelength range was used to examine the optical characteristics of the produced NC. The production of ZnO NPs was verified by recording the distinctive absorbance peak.

2.4.2 Fourier Transform Infrared Spectroscopy

The functional groups involved in the synthesis and stabilization of the NC were identified using FTIR spectroscopy employing the KBr pellet technique. The spectra were recorded within the range of 4000–400 cm^{-1}.

2.4.3 Field Emission Scanning Electron Microscopy

Morphology, particle shape, and particle distribution of the NC were examined using FESEM, JSM-IT800SHL, JEOL, Japan.

2.4.4 Energy-dispersive X-ray Spectroscopy

The elemental composition and purity of the NC were determined using an EDX detector attached to the FESEM instrument.

2.4.5 X-ray Diffraction Analysis

The crystalline structure and phase purity of the NC were analyzed using an X-ray diffractometer (Bruker D8 Advance, Bruker AXS GmbH, Germany) with Cu Kα radiation (λ = 1.5406 Å). At room temperature, the diffraction patterns were captured over a suitable 2θ range.

The average crystallite size (D) was calculated using the Debye–Scherrer equation:

$$D = \frac{0.9\lambda}{\beta \cos\ \theta}$$

where

D = crystallite size (nm),

λ = wavelength of X-ray radiation (1.5406 Å),

β = full width at half maximum (FWHM) in radians, and

θ = Bragg diffraction angle.

The interplanar spacing (d-spacing) was calculated using Bragg's law:

$$d = \frac{\lambda}{2\sin\ \theta}$$

The microstrain (ε) was calculated using:

$$\varepsilon = \frac{\beta}{4\tan\ \theta}$$

The dislocation density (δ), which represents crystal defects, was determined using:

$$\delta = \frac{1}{D^2}$$

These parameters provided detailed information about crystallite size, lattice strain, and structural defects of the synthesized nanocomposites.

2.4.6 Dynamic Light Scattering and Zeta Potential Analysis

The hydrodynamic particle size distribution, PDI, and surface charge (zeta potential) of the synthesized NC were determined using a Bruker DLS instrument equipped with zeta potential measurement capability. Room temperature was used for the measurements. after dispersing the NC in distilled water using ultrasonication.

2.5 Antibacterial Activity

The AA of the synthesized PD-ZnO@P4VP NC was assessed against *K. pneumoniae and S. aureus* using the agar well diffusion method. Fresh bacterial cultures were prepared and uniformly spread onto sterile MHA plates using sterile cotton swabs. Wells of approximately 6 mm diameter were punched aseptically into the agar medium. The PD-ZnO@P4VP NC samples were used at concentrations of 25, 50, and 100 µg/mL, and aqueous plant extract was added to the respective wells. The positive control was amoxicillin, and the negative control was sterile distilled water. Inhibitory zones were measured in mm after the plates were incubated for 24 hours at 37 °C (Santos *et al.* 2023).

2.6 *In Vitro* Cytotoxicity Assay

The cytotoxicity of the PD-ZnO/P4VP NC was evaluated using the MTT assay on HFF-2 (Human Foreskin Fibroblast) cells(Yang *et al.* 2021). HFF-2 cells were seeded into 96-well culture plates and left to adhere overnight in DMEM supplemented with 10% fetal bovine serum and 1% antibiotic–antimycotic solution. The cells were kept in a humidified incubator at 37 °C with 5% CO_2. The cells were then treated with the NC at concentrations of 6.25, 12.5, 25, 50, and 100 µg/mL. Untreated cells served as the control group. Following 24 h of incubation, each well received 5 mg/mL of MTT

solution, which was then incubated for an extra 4 hours. After dissolving the formazan crystals in dimethyl sulfoxide (DMSO), absorbance at 570 nm was measured using a microplate reader.

$$\text{Cell Viability \%} = * 100 \frac{\text{Absorbance of control} - \text{Absorbance of treated}}{\text{Absorbance of control}}$$

Every experiment was conducted in triplicate. The mean ± standard deviation (SD) was used to express the results. Statistical analyses were performed using GraphPad Prism. Differences between groups were analysed using one-way analysis of variance (ANOVA) followed by Tukey's post hoc test. A value of $p < 0.05$ was considered statistically significant.

3. RESULTS AND DISCUSSION

3.1 UV–Visible Spectroscopy

The UV–Visible spectra of the PD extract and synthesized PD-Zn@P4VP NC are shown in Fig.2. The PD extract exhibited a wide absorption in the ultraviolet spectrum due to the presence of phenolic and flavonoid compounds. In contrast, the PD-Zn@P4VP NC displayed a distinct absorption peak at 372 nm, confirming the successful formation of ZnO NPs. The observed absorption band is associated with the characteristic electronic transition of ZnO from the valence band to the conduction band. A nominal optical band-gap value of approximately 3.33 eV can be estimated from the absorption maximum; however, this value is not considered a Tauc-derived band gap, as the raw absorbance data required for Tauc analysis were not available. This absorption corresponds to the characteristic excitonic absorption of ZnO NPs, arising from the valence and conduction band electronic transitions. The slight shift in the absorption peak compared with pure ZnO could be explained by the interaction of ZnO NPs with PD phytochemicals and the P4VP polymer matrix, which enhances NPs stability and reduces aggregation. Similar UV–Visible absorption peaks around 372 nm have been reported for green-synthesized ZnO nanoparticles, confirming the successful formation of crystalline ZnO nanostructures (Byrappa, 2017) Likewise, Singh *et al.* (2023) reported an absorption peak at 367 nm for polymer-functionalized ZnO nanoparticles, demonstrating the successful synthesis of hybrid ZnO nanomaterials with enhanced optical stability. The slight difference in absorption wavelength observed in the present study may be attributed to variations in particle size, surface functionalization, and the interaction between ZnO nanoparticles, *P. daemia* phytochemicals, and the P4VP polymer matrix (Singh *et al.* 2023).

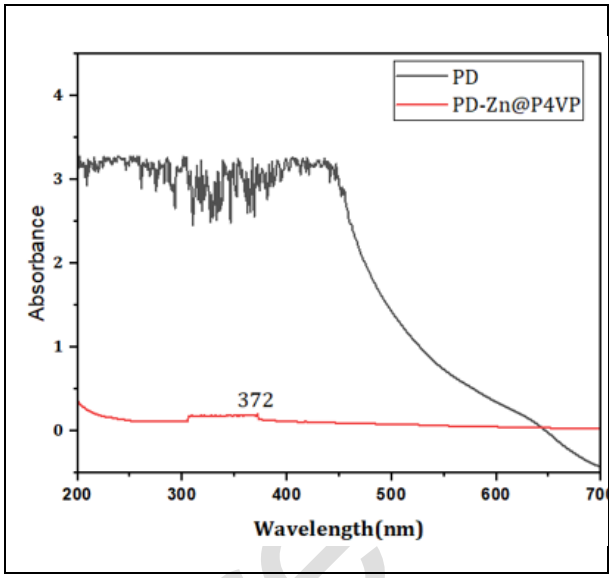

Fig. 2: UV–Visible absorption spectra of *Pergularia daemia* (PD) aqueous extract and the synthesized PD-Zn@P4VP nanocomposite

3.2 SEM and EDX Analysis

The surface morphology of the synthesized PD-Zn@P4VP NC was investigated using FESEM, and the corresponding images are presented in Fig.3A. The NC exhibited irregularly shaped granular NPs with noticeable agglomeration and a rough surface. ImageJ analysis of the FESEM micrographs showed an average particle size of 207 ± 38 nm. The observed aggregation is attributed to the high surface energy of ZnO NPs together with intermolecular interactions between ZnO, bioactive compounds of PD, and the P4VP polymer matrix. Despite the observed aggregation, the particles were distributed throughout the examined regions, suggesting that P4VP and PD-derived phytochemicals provided partial surface stabilization. Similar aggregated yet uniformly distributed morphologies have been reported for green-synthesized polymer-functionalized ZnO nanocomposites, where polymer incorporation improves nanoparticle stability and prevents excessive particle growth (Abdolalian and Taghavijeloudar, 2022).

The elemental composition of the PD-Zn@P4VP NC was confirmed by EDX analysis (Fig.3B). The spectrum exhibited conspicuous peaks that correspond to oxygen (O) and zinc (Zn), indicating that ZnO NPs were successfully formed, while the carbon (C) peak originated from the P4VP polymer backbone and phytocompounds of PD. Quantitative elemental analysis (Table 1) showed weight percentages of 56.3% Zn, 28.1% O, and 15.6% C, with corresponding atomic percentages of 21.9%, 33.1%, and 45.0%, respectively. The presence of carbon is attributed to the polymer matrix and plant-derived organic compounds, whereas the Zn and O peaks confirm the formation of ZnO. The calculated Zn/O atomic ratio (0.66) is consistent with

ZnO nanocomposites containing an organic polymer coating, where the apparent oxygen content is influenced by oxygen-containing phytochemicals and adsorbed surface species. No additional impurity peaks were detected, indicating the absence of detectable additional elemental impurities within the detection limits of EDX. Similar elemental compositions containing only Zn, O, and C have been reported for plant-mediated polymer-functionalized ZnO NCs, confirming successful synthesis and effective surface functionalization.

Table 1: Elemental composition of the PD-Zn@P4VP nanocomposite determined by EDX analysis

Element	Weight (%)	Atomic (%)
Carbon (C)	15.6	45
Oxygen (O)	28.1	33.1
Zinc (Zn)	56.3	21.9
Zn/O atomic ratio	-	0.66

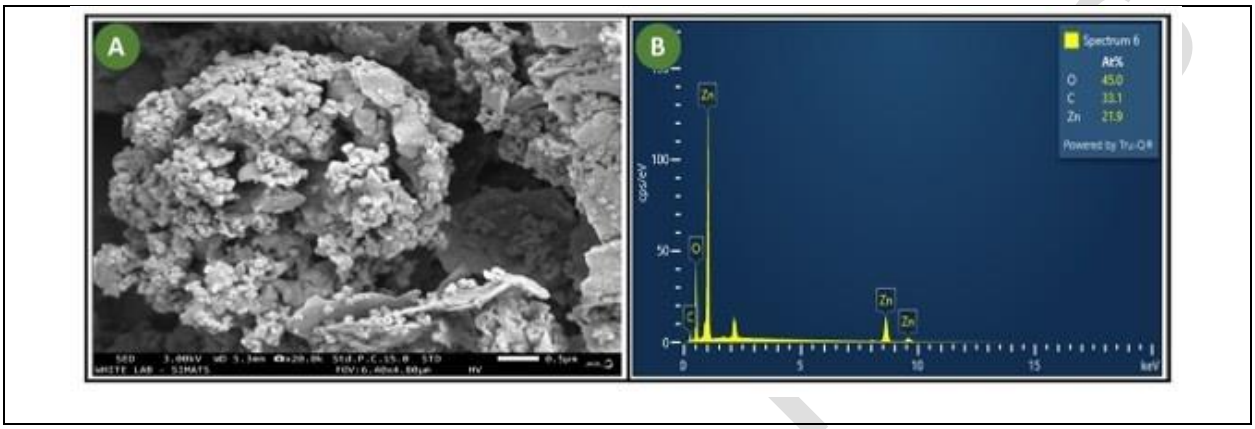

Fig. 3: (A) FESEM micrograph and (B) EDX spectrum of the synthesized PD-Zn@P4VP nanocomposite.

3.3 Fourier Transform Infrared Analysis

The FTIR spectrum of the synthesized PD-Zn@P4VP NC is presented in Fig. 3A, and the characteristic peak assignments are summarized in Table 2. A broad absorption band at 3362 cm^{-1} was assigned to the O–H stretching vibration of hydroxyl groups from phenolic compounds of PD and adsorbed water molecules. The absorption peaks at 3011 and 2931 cm^{-1} correspond to aromatic and aliphatic C–H stretching vibrations associated with the P4VP polymer and phytochemicals(Nguyen *et al.* 2021). The characteristic bands observed at 1552, 1391, and 1334 cm^{-1} were attributed to aromatic C=C stretching and C–N stretching vibrations of the pyridine groups in the P4VP copolymer, indicating successful interaction between the polymer matrix and ZnO NPs (Mohan *et al.* 2023). The absorption band at 1055 cm^{-1} corresponds to C–O stretching vibrations of alcohols and phenolic compounds present in the PD extract. Furthermore, the peaks at 924, 830, and 738 cm^{-1} are assigned to aromatic C–H bending vibrations(Maheshwari and Vijayarengan, 2021).

Most importantly, the absorption bands observed at 674, 615, and 434 cm^{-1} are characteristic of ZnO stretching vibrations, confirming the successful formation of crystalline ZnO NPs (Melegy *et al.* 2025). The coexistence of ZnO bands together with the characteristic functional groups of PD phytochemicals and P4VP polymer demonstrates the successful functionalization of the ZnO nanoparticle surface. The hydroxyl and phenolic groups present in the plant extract interact with Zn^{2+} ions during nanoparticle formation, while the pyridine nitrogen atoms of P4VP coordinate with the ZnO surface, forming an interfacial polymer–ZnO layer around the nanoparticles. This synergistic interaction provides steric and electrostatic stabilization, suppresses nanoparticle aggregation, and improves colloidal stability (Gutul *et al.* 2014). Similar Zn–O stretching bands around 697 cm^{-1} have been reported for polymer-functionalized ZnO nanoparticles, supporting the successful formation and stabilization of ZnO nanostructures (Jovita and Naveen, 2026; Singh *et al.* 2023).

Table 2. FTIR peak assignments of the PD-Zn@P4VP nanocomposite

Wavenumber (cm^{-1})	Functional Group	Assignment
3362	O–H	Hydroxyl stretching of phenolics and adsorbed water
3011	Aromatic C–H	Aromatic C–H stretching
2931	Aliphatic C–H	Aliphatic C–H stretching
1552	C=C	Aromatic ring stretching
1391	C–N	Pyridine group vibration (P4VP)
1334	C–N	Pyridine stretching of P4VP

1055	C–O	Alcohol/phenolic C–O stretching
924	C–H	Aromatic C–H bending
830	C–H	Aromatic C–H bending
738	C–H	Aromatic C–H bending
674	Zn–O	Zn–O stretching vibration
615	Zn–O	Zn–O stretching vibration
434	Zn–O	Zn–O stretching vibration

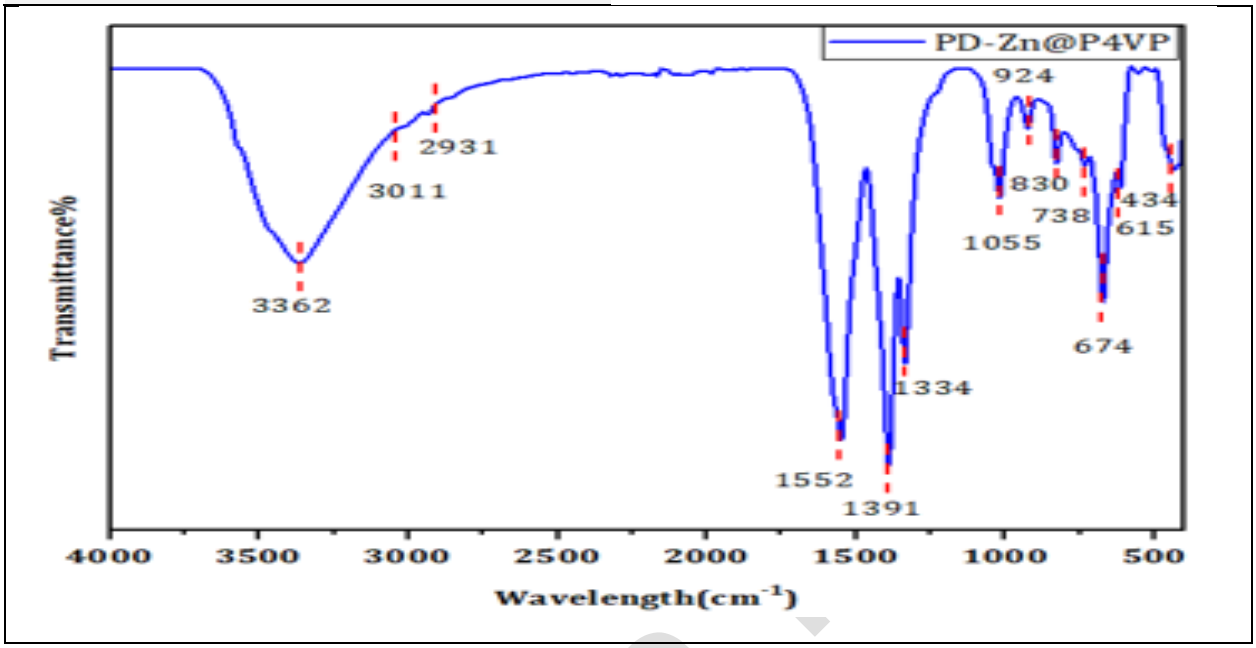

Fig. 4: FTIR spectrum of the synthesized PD-Zn@P4VP nanocomposite

3.4 X-ray Diffraction (XRD) Analysis

The XRD pattern of the synthesized PD-Zn@P4VP NC s presented in Fig.5. The diffraction peaks observed at 31.8°, 34.5°, 36.3°, 47.6°, 56.7°, 63.0°, 66.5°, 68.1°, 69.2°, 72.7° and 77.1° were indexed to the (100), (002), (101), (102), (110), (103), (200), (112), (201),(004) and (202) crystal planes, respectively (Jayswal and Moirangthem, 2018). These reflections match the typical hexagonal wurtzite ZnO crystal structure quite well (JCPDS Card No. 01-075-0576, $P6_3mc$), confirming the successful formation of crystalline ZnO NPs without detectable impurity phases. The crystallite size of the synthesized nanocomposite was estimated using the Debye–Scherrer equation, and the calculated values ranged from 21.03 to 62.02 nm, with an average crystallite size of ~ 28.37 nm (Table 3). The relatively narrow FWHM values (0.285–0.462°) indicate good crystallinity while confirming the nanoscale dimensions of the ZnO crystallites. The absence of additional diffraction peaks further demonstrates the high phase purity of the synthesized nanocomposite, indicating that the incorporation of *Pergularia daemia* phytochemicals and the P4VP polymer did not alter the intrinsic crystal structure of ZnO but instead acted as surface-functionalizing and stabilizing agents.

The calculated lattice parameters were a = 3.25 Å and c = 5.21 Å, yielding a c/a ratio of 1.603, which closely matches the standard values reported for hexagonal wurtzite ZnO (a = 3.249 Å, c = 5.206 Å). This close agreement confirms the preservation of the ZnO crystal lattice after green synthesis and polymer functionalization. Similar diffraction patterns and crystallographic parameters have been reported for plant-mediated ZnO nanoparticles, demonstrating that biomolecules serve primarily as capping and stabilizing agents while maintaining the crystalline integrity of ZnO (Olejnik *et al.* 2021). Overall, the XRD results confirm that the synthesized PD-Zn@P4VP nanocomposite possesses a highly crystalline hexagonal wurtzite ZnO structure with nanoscale crystallite dimensions and high phase purity, characteristics that are beneficial for enhancing its antibacterial performance and physicochemical stability.

Table 3: Crystallographic parameters of the synthesized PD-Zn@P4VP nanocomposite, including 2θ, miller indices (hkl), FWHM, crystallite size, and d-spacing

2θ (°)	Plane (hkl)	FWHM (°)	Crystallite Size (nm)	d-spacing (Å)
31.963	(100)	0.316	26.2	2.79781
34.618	(002)	0.258	32.5	2.58903
36.441	(101)	0.338	24.7	2.46358
47.743	(102)	0.413	21.0	1.90345
56.772	(110)	0.359	25.2	1.62029
63.033	(103)	0.426	21.8	1.47356

66.537	(200)	0.430	22.0	1.40422
68.088	(112)	0.436	21.9	1.37595
69.245	(201)	0.391	24.7	1.35576
72.661	(004)	0.159	64.6	1.30021
77.114	(202)	0.338	30.0	1.23586

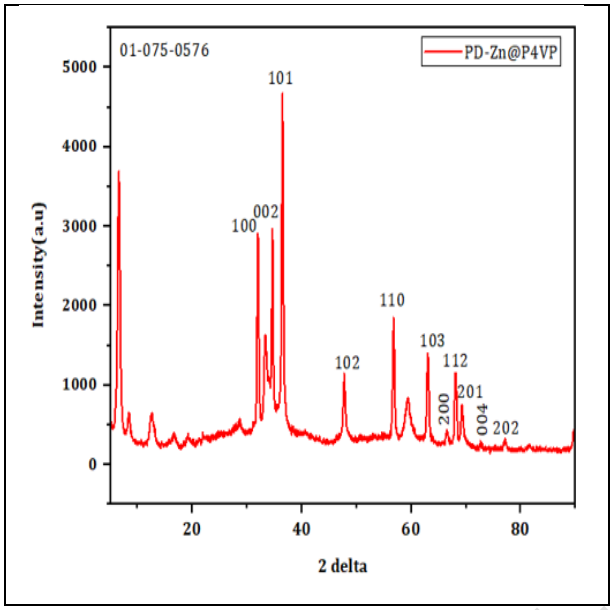

Fig. 5: X-ray diffraction (XRD) pattern of the synthesized PD-Zn@P4VP nanocomposite

3.5 Dynamic Light Scattering and Zeta Potential Analysis

The surface charge and hydrodynamic particle size of the PD-Zn@P4VP NC were determined by DLS and zeta potential analysis as shown in Fig.6 (A-D). The DLS analysis revealed an average hydrodynamic particle size of 280.8 nm with the PDI of 0.4447 indicates a moderately polydisperse particle population. The larger hydrodynamic diameter compared with the FESEM-derived size of 207 ± 38 nm can be attributed to hydration of the nanoparticles and the presence of the surrounding P4VP/biomolecular layer in aqueous suspension. The PDI of 0.4447 indicates a moderately broad particle-size distribution and suggests some degree of particle association in suspension. This difference is expected because FESEM measures dried particles, whereas DLS measures their effective hydrodynamic diameter in a hydrated state. Compared with previously reported ZnO nanoparticles (449.8 nm; PDI 0.21), the present NC exhibited a smaller hydrodynamic size, although its higher PDI indicates greater size heterogeneity(Srivastav *et al.* 2016).

The zeta potential of the PD-Zn@P4VP NC was 32.15 mV, indicating good colloidal stability. Generally, nanoparticles with absolute zeta potential values greater than ±30 mV are considered highly stable because sufficient electrostatic repulsion prevents particle aggregation. In addition, the adsorption of P4VP polymer chains and PD phytochemicals on the ZnO nanoparticle surface provides steric stabilization, further enhancing dispersion stability in aqueous media. The combined electrostatic and steric stabilization is expected to improve the suspension stability of the nanocomposite during biological applications. These findings are consistent with previous reports demonstrating that polymer-coated metal oxide nanoparticles exhibit increased hydrodynamic size and improved colloidal stability due to polymer hydration and effective surface capping (Briffa *et al.* 2017)

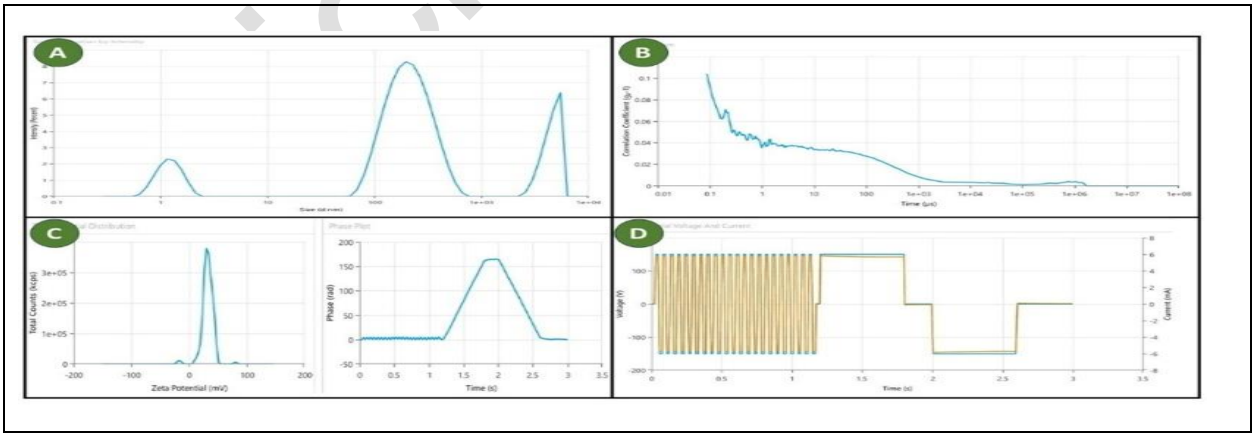

Fig. 6: Dynamic light scattering (DLS) particle-size distribution and zeta-potential analysis of the synthesized PD-Zn@P4VP nanocomposite

3.6 Antibacterial Activity

The AA of the synthesized PD-Zn@P4VP NC against *Staphylococcus aureus* and *Klebsiella pneumoniae* was evaluated using the agar well diffusion method is presented in Fig.7. The NC exhibited concentration-dependent AA against both bacterial strains. At 25, 50, and 100 µg/mL, the inhibition zones

against *S. aureus* were 13, 14, and 19 mm, respectively, while the plant extract alone produced an inhibition zone of 12 mm. Similarly, against *K. pneumoniae*, inhibition zones of 14, 16, and 20 mm were observed for the NC, compared with 13 mm for the plant extract. The positive control, amoxicillin shown inhibition zones of 19 mm against *S. aureus* and 13 mm against *K. pneumoniae*. These results demonstrate that the PD-Zn@P4VP NC exhibited enhanced AA compared with the PD extract alone, particularly at the 100µg/mL highest concentration. The observed antibacterial activity may be attributed to the combined contribution of ZnO, PD-derived phytochemicals, and P4VP-mediated nanoparticle stabilization and dispersion. Based on previously reported mechanisms of ZnO nanoparticles, their antibacterial effects may involve ROS generation, Zn^{2+} release, and disruption of bacterial membrane integrity. Similarly, phenolic and flavonoid constituents of *P. daemia* may contribute to membrane perturbation and interference with bacterial metabolic processes. However, these mechanisms were not directly investigated in the present study; therefore, they are considered possible mechanisms rather than experimentally confirmed pathways. In addition, because separate ZnO-only and P4VP-only controls were not included in the original experimental design, a synergistic interaction cannot be conclusively established. Therefore, the antibacterial effect is conservatively interpreted as an enhanced or combined effect of the components (Masadeh *et al.* 2025; Okaiyeto *et al.* 2024).

The present findings are consistent with previous reports demonstrating the potent AA of ZnO NPs through ROS-mediated membrane damage and oxidative stress. Similarly, *Pergularia daemia* leaf extracts have been reported to inhibit *Staphylococcus aureus*, *Bacillus subtilis*, and *Proteus vulgaris*, with inhibition zones ranging from 15–20 mm (Savarimuthu *et al.* 2008; Tiwari *et al.* 2018). The present results therefore demonstrate the *in vitro* antibacterial potential of the synthesized PD-Zn@P4VP NC. Further mechanistic studies involving direct measurement of ROS generation, Zn^{2+} release, membrane integrity, and bacterial cell damage, together with individual-component controls, are required to confirm the proposed antibacterial mechanisms and establish whether any synergistic interaction occurs.

Fig. 7: Antibacterial activity of the PD-Zn@P4VP nanocomposite against *Staphylococcus aureus* and *Klebsiella pneumoniae* at different concentrations

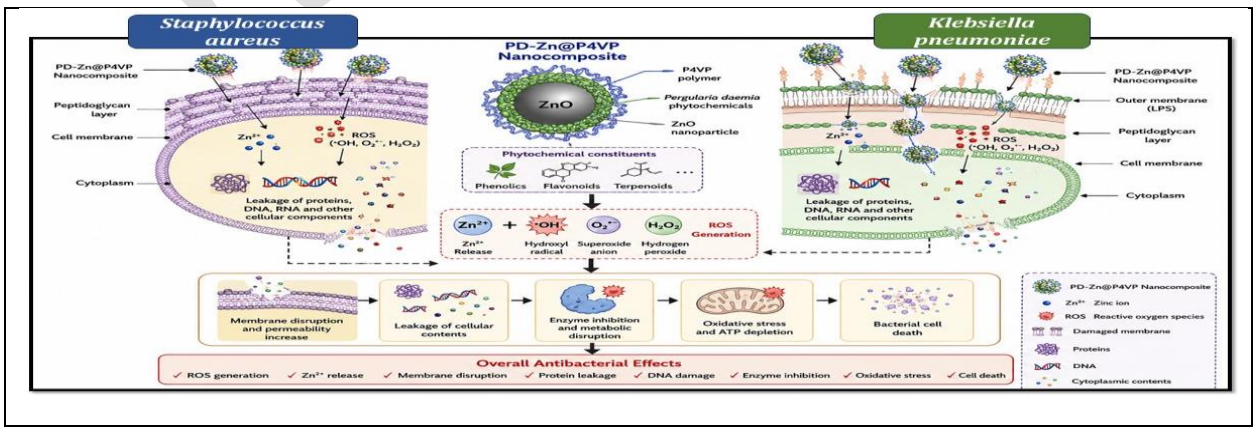

Fig. 8: Proposed antibacterial mechanism of the PD-Zn@P4VP nanocomposite against *Staphylococcus aureus* and *Klebsiella pneumoniae*

3.7 *In Vitro* Cytotoxicity Evaluation

The cytotoxicity of the synthesized PD-Zn@P4VP NC was evaluated against HFF-2 normal human fibroblast cells using the MTT assay and is presented in Fig.9. The NC exhibited a concentration-dependent reduction in cell viability. Compared with the untreated control (100%), cell viability remained ~ 95%, 91%, 88%, 77%, and 69% following treatment with 6.25, 12.5, 25, 50, and 100 µg/mL, respectively. Statistical analysis was performed using one-way ANOVA followed by Tukey's multiple-comparison test. The reductions observed at 6.25 and 12.5 µg/mL were not statistically significant ($p > 0.05$), whereas significant reductions were observed at 25 and 50 µg/mL (**$p < 0.01$) and at 100 µg/mL (*$p < 0.05$) compared with the untreated control. Nevertheless, approximately 69% of cells remained viable at the highest concentration tested, indicating moderate cytocompatibility under the specific *in vitro* conditions and concentration range investigated, rather than demonstrating complete cellular safety.

The concentration-dependent reduction in viability is consistent with previous reports on ZnO NPs, in which increasing exposure concentrations can promote intracellular reactive oxygen species generation, oxidative stress, and mitochondrial dysfunction. The relatively higher viability observed at lower concentrations in the present study may be associated with surface functionalization by PD-derived phytochemicals and stabilization by P4VP, which could influence nanoparticle–cell interactions and reduce direct cellular exposure to the ZnO surface. However, this interpretation requires further mechanistic investigation because ROS generation, mitochondrial function, apoptosis, and cellular uptake were not directly evaluated in the present study. Therefore, the present findings demonstrate concentration-dependent cytotoxic effects with comparatively higher cell viability at lower concentrations, but they should not be interpreted as definitive evidence of long-term biomedical safety (Król-Górniak *et al.* 2021). Since only normal HFF-2 fibroblasts were evaluated, further studies involving multiple normal and disease-relevant cell lines, mechanistic assays, and *in vivo* biocompatibility studies are required to establish the broader biological safety profile of PD-Zn@P4VP NC.

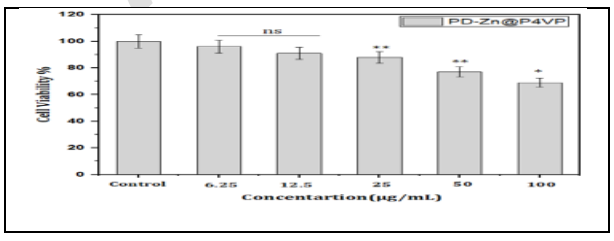

Fig. 9: Cell viability of HFF-2 fibroblast cells treated with different concentrations of the PD-Zn@P4VP nanocomposite, as determined by the MTT assay

Data are presented as mean ± SD (n = 3). Statistical significance was evaluated using one-way ANOVA followed by Tukey's multiple-comparison test. ns, $p > 0.05$; *$p < 0.05$; **$p < 0.01$; ***$p < 0.001$ compared with the untreated control.

3.8 Morphological Evaluation of HFF-2 Cells

The morphological changes in HFF-2 cells following treatment with PD-Zn@P4VP NC were examined under an inverted microscope Fig.9. Untreated control cells displayed normal spindle-shaped morphology with uniform distribution and strong adherence to the culture surface. Cells treated with 6.25–25 µg/mL retained their characteristic fibroblast morphology with minimal morphological alterations, indicating good biocompatibility at lower concentrations. At higher concentrations (50 and 100 µg/mL), a slight decrease in cell density, together with mild cell shrinkage and rounding, was observed. Nevertheless, most cells remained attached to the culture surface and retained their overall structural integrity. These qualitative morphological observations were consistent with the concentration-dependent MTT results. These observations correlate well with the MTT assay results and indicate that the synthesized NC exhibits acceptable compatibility with normal cells while retaining its biological activity. The findings are further supported by previous studies demonstrating that PD extracts possess a high safety, with no significant toxicity observed in acute toxicity studies up to 2500 mg/kg in experimental animals (Vaithiyanathan and Mirunalini, 2015). In addition, methanolic extracts of PD have been reported to induce concentration-dependent cytotoxicity in MDA-MB-231 breast cancer cells while exhibiting comparatively lower toxicity toward normal cells, highlighting the selective biological potential of the plant phytochemicals (GH *et al.* 2023). The MTT assay demonstrated that the PD-Zn@P4VP NC exhibited acceptable cytocompatibility toward HFF-2 normal fibroblast cells, with approximately 69% cell viability maintained even at the highest tested concentration (100 µg/mL), indicating relatively low toxicity toward normal cells.

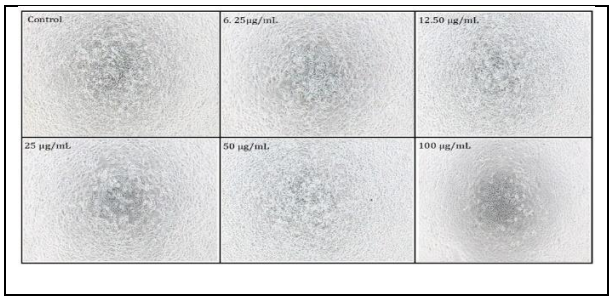

Fig. 10: Representative inverted-microscope images showing the morphological changes in HFF-2 fibroblast cells following treatment with different concentrations of the PD-Zn@P4VP nanocomposite

4. CONCLUSIONS

In the present study, PD-Zn@P4VP NC was successfully synthesized using a green and environmentally friendly approach. The successful formation of the NC was confirmed by UV–Visible spectroscopy, FTIR, FESEM–EDX, XRD, DLS, and zeta potential analyses. The nanocomposite exhibited a characteristic UV absorbance peak at 372 nm, a crystalline hexagonal wurtzite ZnO structure, good colloidal stability and successful surface functionalization by *P. daemia* phytochemicals and the P4VP polymer. The PD-Zn@P4VP NC exhibited concentration-dependent AA against *Staphylococcus aureus* and *Klebsiella pneumoniae* and acceptable cytocompatibility toward HFF-2 normal fibroblast cells,with ~ 69% cell viability maintained at the highest tested concentration (100 µg/mL). These findings provide preliminary *in-vitro* evidence of antibacterial activity and compatibility with normal fibroblasts under the tested conditions. The novelty of this study lies in the green synthesis of a *P. daemia*-functionalized ZnO/P4VP nanocomposite and its comprehensive physicochemical characterization together with antibacterial and cytocompatibility evaluation. However, the study is limited to *in-vitro* antibacterial testing and cytocompatibility assessment using a normal fibroblast cell line. Further investigations involving relevant cancer cell lines, in vivo biocompatibility and wound-healing studies, drug-delivery evaluation, long-term physicochemical stability, and detailed mechanistic studies are required to determine the broader biological applicability of the nanocomposite.

AUTHOR CONTRIBUTIONS

S. S. Sandeep: Conceptualization, Methodology, Investigation, Writing – original draft. G. Pallavi: Validation, Formal analysis, Data curation, Software. S. Revathi: Supervision, Project administration, Resources, Funding acquisition, Writing – review & editing. All authors have read and agreed to the published version of the manuscript.

AVAILABILITY OF DATA AND MATERIALS

All data generated or analyzed during this study are included in this published article.

ACKNOWLEDGMENT

he authors thank the management of SIMATS, Chennai, for providing the necessary infrastructure and support to carry out this research work.

FUNDING

This research received no specific grant from any funding agency in the public, commercial, or not-for-profit sectors.

CONFLICTS OF INTEREST

The authors declare that there is no conflict of interest.

COPYRIGHT

REFERENCE

Abdolalian, S. and Taghavijeloudar, M., Performance evaluation and optimization of ZnO-PVP nanoparticles for photocatalytic wastewater treatment: Interactions between UV light intensity and nanoparticles dosage, *J. Clean. Prod.*, 365(132833), 132833 (2022). https://doi.org/10.1016/j.jclepro.2022.132833

Ahmed, S. K., Hussein, S., Qurbani, K., Ibrahim, R. H., Fareeq, A., Mahmood, K. A. and Mohamed, M. G., Antimicrobial resistance: Impacts, challenges, and future prospects, *J. Med. Surg. Pub. Health.*, 2, 100081 (2024). https://doi.org/10.1016/j.glmedi.2024.100081

Ananth, D. A., Deviram, G., Mahalakshmi, V. and Bharathi, V. R., Active status on phytochemistry and pharmacology of Pergularia daemia Forsk. (Trellis-vine): a review, *Clin. Phytosci.*, 7(1), 60(2021). https://doi.org/10.1186/s40816-021-00295-z

Ananth, D. A., Rameshkumar, A., Jeyadevi, R., Aseervatham, G. S. B., Sripriya, J., Bose, P. C. and Sivasudha, T., Amelioratory effect of flavonoids rich Pergularia daemia extract against CFA induced arthritic rats, *Biomed. Pharmacother.*, 80, 244–252(2016). https://doi.org/10.1016/j.biopha.2016.03.019

Briffa, S. M., Lynch, I., Trouillet, V., Bruns, M., Hapiuk, D., Liu, J., Palmer, R. E. and Valsami-Jones, E., Development of scalable and versatile nanomaterial libraries for nanosafety studies: polyvinylpyrrolidone (PVP) capped metal oxide nanoparticles, *RSC Adv.*, 7(7), 3894–3906 (2017). https://doi.org/10.1039/c6ra25064e

Byrappa, K., Use of honey in stabilization of ZnO nanoparticles synthesized via hydrothermal route and assessment of their antibacterial activity and cytotoxicity, *Glob. J. Nanomed.*, 2(2), (2017). https://doi.org/10.19080/gjn.2017.02.555585

Constantino, V. R. L., Figueiredo, M. P., Magri, V. R., Eulálio, D., Cunha, V. R. R., Alcântara, A. C. S. and Perotti, G. F., Biomaterials based on organic polymers and layered double hydroxides nanocomposites: Drug delivery and tissue engineering, *Pharma.*, 15(2), 413 (2023). https://doi.org/10.3390/pharmaceutics15020413

Dada, K. S., Olekhnovich, R. O. and Zaripova, F. F., Review of polymers and nanocomposites based on hyaluronic acid and zinc oxide nanoparticles in synthesizing microneedles for transdermal drug delivery, *Polym.*, 18(2), 217 (2026). https://doi.org/10.3390/polym18020217

Ehisuoria, C. O., Iyekowa, O., Okieimen, F. E. and Okodugha, D. O., Antioxidant Potentials of Canna indica, Pergularia daemia, and Parquetina nigrescens leaves, *J. Chem. Soc. Niger.*, 50(6), 1193–1199 (2025). https://doi.org/10.4314/jcsn.v50i6.5

Elshobary, M. E., Badawy, N. K., Ashraf, Y., Zatioun, A. A., Masriya, H. H., Ammar, M. M., Mohamed, N. A., Mourad, S. and Assy, A. M., Combating antibiotic resistance: Mechanisms, multidrug-resistant pathogens, and novel therapeutic approaches: An updated review, *Pharma.*, 18(3), 402 (2025). https://doi.org/10.3390/ph18030402

Elumalai, M., Nagaraj, G., Kasthuri, J., Vellaichamy, E. and Rajendiran, N., Evaluation of cytotoxic activity against A549 human lung cancer cells using green synthesized N-Cholyl D-Penicillamine encapsulated silver and gold nanoparticles, *Inorg. Chem. Commun.*, 153, 110834 (2023). https://doi.org/10.1016/j.inoche.2023.110834

Gal, Y. S., Lee, W. C., Jin, S. H., Lyoo, W. S., Kim, S. H., Park, J. W. and Lim, K. T., Synthesis and properties of poly(4-vinylpyridine-co-styrene) with pendant azobenzonitrile moieties, *J. Nanosci. Nanotechnol.*, 11(5), 4611–4614 (2011). https://doi.org/10.1166/jnn.2011.3677

GH, Akhil, B. J., Kariyil, G. A., Desai, R., John, S. V. V., Bhat, A. and Dhabholkar., Methanol extract of Pergularia daemia (Forssk.) Chiov. leaves induce apoptosis in triple-negative breast cancer through intrinsic pathway, *Indian J. Exp. Biol.*, 61(5), (2023). https://doi.org/10.56042/ijeb.v61i05.850

Gutul, T., Rusu, E., Condur, N., Ursaki, V., Goncearenco, E. and Vlazan, P., Preparation of poly(N-vinylpyrrolidone)-stabilized ZnO colloid nanoparticles, *Beilstein J. Nanotechnol.*, 5, 402–406 (2014). https://doi.org/10.3762/bjnano.5.47

Herin, R. F., Judit, A. S. S., Sebastiammal, S., Shabna, S., Dhas, S. S. J. and Biju, C. S., Functionalized ZnO NPs and biopolymers-coated ZnO NPs for drug delivery and biomedical applications—A review, *Regen. Eng. Transl. Med.*, 11(1), 165–189 (2025). https://doi.org/10.1007/s40883-024-00354-0

Hetta, H. F., Ramadan, Y. N., Al-Harbi, A. I., A Ahmed, E., Battah, B., Abd Ellah, N. H., Zanetti, S. and Donadu, M. G., Nanotechnology as a promising approach to combat multidrug resistant bacteria: A comprehensive review and future perspectives, *Biomed.*, 11(2), 413 (2023). https://doi.org/10.3390/biomedicines11020413

Jayswal, S. and Moirangthem, R. S., Thermal decomposition route to synthesize ZnO nanoparticles for photocatalytic application, *AIP Conf. Proc.*, 2009, 020023(2018). https://doi.org/10.1063/1.5052092

Jovita, S. and Naveen, C., Bioactive ZnS-reinforced Gellan Gum film enriched with Cucumis maderaspatanus L. blend membrane for antimicrobial application, *South Afr. J. Bot.*, 195, 58–65 (2026). https://doi.org/10.1016/j.sajb.2026.05.003

Kavaye, K. A., Okomolo, M. F. C., Omam, O. J. P., Mbomo, A. R. E., Ojong, L. and Ngo, B. E., Pergularia daemia alters epileptogenesis and attenuates cognitive impairment in kainate-treated mice: Insight into anti-inflammatory mechanisms, *Epilepsy Behav.*, 115, 107707 (2021). https://doi.org/10.1016/j.yebeh.2020.107707

Król-Górniak, A., Rafińska, K., Monedeiro, F., Pomastowski, P. and Buszewski, B., Comparison study of cytotoxicity of bare and functionalized zinc oxide nanoparticles, *Int. J. Mol. Sci.*, 22(17), 9529 (2021). https://doi.org/10.3390/ijms22179529

Maheshwari, M. and Vijayarengan, P., Phytochemical evaluation, FT-IR and GC-MS analysis of leaf extracts of Pergularia daemia, *Nat. Environ. Pollut. Technol.*, 20(1), 259–265 (2021). https://doi.org/10.46488/nept.2021.v20i01.028

Masadeh, M. M., Bany-Ali, N. M., Khanfar, M. S., Alzoubi, K. H., Masadeh, M. M. and Al Momany, E. M., Synergistic antibacterial effect of ZnO nanoparticles and antibiotics against multidrug-resistant biofilm bacteria, *Curr. Drug Deliv.*, 22(1), 92–106 (2025). https://doi.org/10.2174/0115672018279213240110045557

Melegy, A. A., Abdel-Monem, Y. K., Ali, F. A., Maysour, N. E. and Atta, A. M., Superparamagnetic Fe_3O_4/ZnO/$ZnFe_2O_4$ nanocomposites for efficient photocatalytic degradation of methylene blue from water under UV light, *Sci. Rep.*, 15(1), 40393 (2025). https://doi.org/10.1038/s41598-025-24533-3

Mohan, S., Sudarsan, S., Parthiban, E., Guhanathan, S. and Prasad, S. V. S., Synthesis and characterization of binding interaction of ZnO nanoparticles with organic compounds, *Mater. Today Proc.*, 8631(2023). https://doi.org/10.1016/j.matpr.2023.03.791

Nguyen, L. T., Pham, H. Q., Nguyen, D. A. S., Nguyen, L. T., Huynh, K. P. H., Le Tran, H., Mai, P. T., Nguyen, H. T., Nguyen, L. T. T. and Truong, T. T., 10-(pyren-1-yl)-10h-phenothiazine and pyrene as organic catalysts for photoinitiated ATRP of 4-

vinylpyridine, *Polímeros.*, 31(1), e2021001(2021). https://doi.org/10.1590/0104-1428.08120

Okaiyeto, K., Gigliobianco, M. R. and Di Martino, P., Biogenic zinc oxide nanoparticles as a promising antibacterial agent: Synthesis and characterization, *Int. J. Mol. Sci.*, 25(17), 9500 (2024). https://doi.org/10.3390/ijms25179500

Olejnik, M., Kersting, M., Rosenkranz, N., Loza, K., Breisch, M., Rostek, A., Prymak, O., Schürmeyer, L., Westphal, G., Köller, M., Bünger, J., Epple, M. and Sengstock, C., Cell-biological effects of zinc oxide spheres and rods from the nano- to the microscale at sub-toxic levels, *Cell Biol. Toxicol.*, 37(4), 573–593 (2021). https://doi.org/10.1007/s10565-020-09571-z

Ramachandran, M., Deepika, N. and Jayakumar, M.,Toxicity of Ocimum americanum L. extracts against Aedes aegypti larvae (Diptera: Culicidae) and their impact on insecticide resistance, *Arch. Insect Biochem. Physiol.*, 113(1), e21961 (2023). https://doi.org/10.1002/arch.21961

Santos, C. F., Andrade, S. M., Mil-Homens, D., Montemor, M. F. and Alves, M. M., Antibacterial activity of ZnO nanoparticles in a *Staphylococcus aureus*-infected *Galleria mellonella* model is tuned by different apple-derived phytocargos, *J. Funct. Biomater.*, 14(9), 463 (2023). https://doi.org/10.3390/jfb14090463

Savarimuthu, I., Pavunraj, M., Veeramuthu, D., Raja, N. and Muthu, C., Antibacterial activity of a novel quinone from the leaves of Pergularia daemia (Forsk.), a traditional medicinal plant, *Asian J. Tradit. Med.*, 4(1), (2009).

Sharma, P., Jang, N. Y., Lee, J. W., Park, B. C., Kim, Y. K. and Cho, N. H., Application of ZnO-based nanocomposites for vaccines and cancer immunotherapy, *Pharma.*, 11(10), E493 (2019). https://doi.org/10.3390/pharmaceutics11100493

Sidhic, J., Aswathi, M. K., Prasad, A., Tom, A., Mohan, P., Sarbadhikary, P., Narayanankutty, A., George, S., Abrahamse, H. and George, B. P., Advancements in metal and metal oxide nanoparticles for targeted cancer therapy and imaging: Mechanisms, applications, and safety concerns, *J. Drug Deliv. Sci. Technol.*, 105, 106622 (2025). https://doi.org/10.1016/j.jddst.2025.106622

Singh, K., Nancy, Bhattu, M., Singh, G., Mubarak, N. M. and Singh, J., Light-absorption-driven photocatalysis and antimicrobial potential of PVP-capped zinc oxide nanoparticles, *Sci. Rep.*, 13(1), 13886 (2023). https://doi.org/10.1038/s41598-023-41103-7

Song, T., Qu, Y., Ren, Z., Yu, S., Sun, M., Yu, X. and Yu, X., Synthesis and characterization of polyvinylpyrrolidone-modified ZnO quantum dots and their in vitro photodynamic tumor suppressive action, *Int. J. Mol. Sci.*, 22(15), 8106 (2021). https://doi.org/10.3390/ijms22158106

Srivastav, A. K., Kumar, M., Ansari, N. G., Jain, A. K., Shankar, J., Arjaria, N., Jagdale, P. and Singh, D., A comprehensive toxicity study of zinc oxide nanoparticles versus their bulk in Wistar rats: Toxicity study of zinc oxide nanoparticles, *Hum. Exp. Toxicol.*, 35(12), 1286–1304(2016). https://doi.org/10.1177/0960327116629530

Tiwari, V., Mishra, N., Gadani, K., Solanki, P. S., Shah, N. A. and Tiwari, M., Mechanism of anti-bacterial activity of zinc oxide nanoparticle against carbapenem-resistant Acinetobacter baumannii, *Front. Microbiol.*, 9, 1218 (2018). https://doi.org/10.3389/fmicb.2018.01218

Vagena, I. A., Gatou, M. A., Theocharous, G., Pantelis, P., Gazouli, M., Pippa, N., Gorgoulis, V. G., Pavlatou, E. A. and Lagopati, N., Functionalized ZnO-based nanocomposites for diverse biological applications: Current trends and future perspectives, *Nanomater.*, 14(5), 397 (2024). https://doi.org/10.3390/nano14050397

Vaithiyanathan, V. and Mirunalini, S., Assessment of antioxidant potential and acute toxicity studies of whole plant extract of Pergularia daemia (forsk), *Toxicol. Int.*, 22(1), 54–60 (2015). https://doi.org/10.4103/0971-6580.172257

Xie, J., Li, H., Zhang, T., Song, B., Wang, X. and Gu, Z., Recent advances in ZnO nanomaterial-mediated biological applications and action mechanisms, *Nanomater.*, 13(9), 1500 (2023). https://doi.org/10.3390/nano13091500

Yang, Y., Deng, G., Wang, P., Lv, G., Mao, R., Sun, Y., Wang, B., Liu, X., Bian, L. and Zhou, D., A selenium nanocomposite protects the mouse brain from oxidative injury following intracerebral hemorrhage, *Int. J. Nanomed.*, 16, 775–788 (2021). https://doi.org/10.2147/IJN.S293681

Zafar, A., Khatoon, S., Khan, M. J., Abu, J. and Naeem, A., Advancements and limitations in traditional anti-cancer therapies: a comprehensive review of surgery, chemotherapy, radiation therapy, and hormonal therapy, *Discov. Oncol.*, 16(1), 607 (2025). https://doi.org/10.1007/s12672-025-02198-8